Ceram. Trans., **159**, 219-229 (2004)

SYNTHESIS OF A BARIUM SULFATE NANOPARTICLE CONTRAST AGENT FOR MICRO-COMPUTED TOMOGRAPHY OF BONE MICROSTRUCTURE

Huijie Leng, Xiang Wang, Glen L. Niebur and Ryan K. Roeder
University of Notre Dame
Department of Aerospace and Mechanical Engineering
Notre Dame, IN 46556

ABSTRACT

A noninvasive, three-dimensional technique is needed to image microstructural features – such as microcracks and vasculature – in bone tissue. Micro-computed tomography (μCT) using a radiopaque barium sulfate contrast agent to label microstructural features in bone tissue has been proposed. The size of vasculature and microcracks in bone tissue requires nano-scale barium sulfate particles. Therefore, a simple aqueous precipitation method was used to synthesize barium sulfate particles less than 100 nm in size. The effects of the reagent solution concentration, molar ratio, feeding order, feeding speed and pH were investigated. Finally, the feasibility of imaging the synthesized barium sulfate nanoparticles in μCT was verified. The detected signal due to barium sulfate nanoparticles was amplified by a volumetric factor of nearly eight, which enabled detection of features much smaller than the nominal resolution of the instrument.

INTRODUCTION

Microdamage in bone tissue is caused by fatigue, creep, or monotonic overloading.[1] Accumulation of microdamage leads to a degradation of mechanical properties and an increased risk of fracture, including stress fractures in athletes and bone fragility in the elderly.[2-4] In human cortical bone, microdamage accumulates in the form of microcracks[5,6] and degradation of the elastic modulus is dependent on the applied stress state.[7,8] Therefore, quantitative measurement of the distribution and orientation of microcracks is important in order to assess the effects of microdamage on the mechanical behavior of bone tissue.

Microdamage in bone is currently imaged by optical microscopy using various epifluorescent contrast agents which chelate to calcium exposed at a free surface, such as a microcrack.[9-11] Sequential staining with multiple contrast agents can be used to differentiate microdamage from other microstructural features, as well as different damage events.[6,10,11] While bone tissue may be stained *en bloc*, quantitative measurements require the preparation of many histologic sections. Thus, these methods are inherently invasive and two-dimensional, and a non-invasive, three-dimensional technique is needed for imaging microdamage in bone. Micro-computed tomography (μCT) has been proposed for such a technique, using a suitable contrast agent.

In order for μCT to differentiate microcracks from bone, a contrast agent which is much more radiopaque than bone tissue must be used to selectively label microcracks. In practice, after staining with the contrast agent, microcracks would be detected as bright features in μCT images.

Barium sulfate ($BaSO_4$) is a logical choice for the contrast agent due to current clinical use as a contrast agent for conventional radiography of the digestive tract and a radiopaque filler in commercial bone cement. Thus, the biocompatibility of barium sulfate is reasonably well accepted. Typical microcracks in cortical bone tissue are 30-100 μm in length and less than one μm in width.[1,12,13] Therefore, in order to be used as a contrast agent for microcracks in cortical bone tissue, barium sulfate nanoparticles are required.

Barium sulfate precipitation has received significant attention in the literature, not only due to the industrial significance of scaling, but also as a model system for precipitation investigations.[15-24] Barium chloride and sodium sulfate are usually chosen as the reagents to study precipitation of barium sulfate. In some cases, sulfuric acid[15,21] or potassium sulfate[18-20] are also used. The size and morphology of any precipitated crystal is governed by the thermodynamics and kinetics of nucleation and growth.[25] Taguchi *et al.*[16] evaluated the nucleation and growth kinetics of barium sulfate for equimolar amounts of barium and sulfate ions, and Aoun *et al.*[18] studied the kinetics of barium sulfate precipitation with a molar excess of either barium or sulfate ions. Wong *et al.*[24] showed that a considerable excess of either reagent solution produced the smallest particles but the particles were all on the micro-scale.

Many methods and modifications have been used to control the size and morphology of precipitated barium sulfate, such as the addition of various additives,[21,26-28] chelate decomposition,[29] and microemulsions.[30-32] The use of additives, including chelating agents, has shown the greatest influence on particle morphology, but particle sizes have typically remained greater than nano-scale. Microemulsions also enable particle size control by varying the molar ratio of water to surfactant, but the uniformity of precipitates is more difficult to control and the yield is relatively small.

The objective of this work was to synthesize barium sulfate nanoparticles suitable for use as a contrast agent for μCT. Precipitation experiments focused on identifying key parameters for precipitating equiaxed nanoparticles. Finally, the feasibility of imaging the synthesized barium sulfate nanoparticles using μCT was investigated.

EXPERIMENTAL METHODS

Synthesis of Barium Sulfate Nanoparticles

Barium sulfate was precipitated instantaneously by mixing aqueous solutions of barium chloride and sodium sulfate as

$$BaCl_2 + Na_2SO_4 \rightarrow BaSO_4\downarrow + 2NaCl \qquad (1)$$

Barium chloride (Certified ACS crystal, Fisher Scientific, Fair Lawn, NJ) and sodium sulfate (anhydrous powder, Fisher Scientific, Fair Lawn, NJ) solutions were prepared by dissolving the desired concentration of reagents in de-ionized water. The pH of all reagent solutions was adjusted using nitric acid (ACS reagent, Aldrich Chemical Co., Milwaukee, WI) and sodium hydroxide (ACS reagent, Sigma Chemical Co., St. Louis, MO). Precipitation occurred as the feeding reagent solution was dropped into the other reagent solution using a buret to control the

feeding rate. The mixed reagent solution was kept at ambient temperature and stirred at a constant speed of 450 rpm using a magnetic stir plate. Barium sulfate precipitates were collected by centrifugation at 4500 rpm for 20 min. Precipitates were washed with de-ionized water and recollected three times. Collected precipitates were dried in an oven at 40°C for more than 24 h.

Experiments were designed to study the effects of independent parameters on the size and morphology of precipitates. Experimental parameters included the reagent solution concentration, molar ratio, feeding order, feeding speed and pH. All experimental conditions are shown in Table I.

Powder x-ray diffraction (XRD) (X1 Advanced Diffraction System, Scintag, Inc., Sunnyvale, CA) was performed to verify the phase of the precipitated crystals. Powders were examined over 15-50° with a step size of 0.02° and a step time of 0.5 s, using Cu Kα radiation generated at 40 kV and 30 mA. The size and morphology of precipitates was examined qualitatively using field emission scanning electron microscopy (FESEM). For each sample, 0.003 g of precipitates was added to 1 ml methanol and dispersed in a sonic bath for 10 min. The suspension was dropped onto a sample holder and the methanol evaporated in air. After drying, samples were coated with gold and examined by FESEM (S-4500, Hitachi High-Technologies Corporation, Tokyo, Japan) with an accelerating voltage of 25 kV and working distance of 7 mm. The mean size of nanoparticles was also quantified by XRD line broadening measurements using the Scherrer equation and Warren's method.[33] The (200), (020) and (002) reflections were each scanned with a step size of 0.01° and a step time of 2.0 s, and fit with a Pearson 7 function using a freeware software package (MacDiff 4.2).

Table I. Experimental parameters investigated for barium sulfate precipitation.

Experiment	$[Ba^{2+}]$	$[SO_4^{2-}]$	$[Ba^{2+}]/[SO_4^{2-}]$	Feeding reagent	pH	Feeding speed
1	0.55 M	0.55 M	1.0	SO_4^{2-}	7	2.5 ml/min
2	0.01 M	0.01 M	1.0	SO_4^{2-}	7	2.5 ml/min
3	0.10 M	1.00 M	0.1	SO_4^{2-}	7	2.5 ml/min
4	1.00 M	0.10 M	10	SO_4^{2-}	7	2.5 ml/min
5	0.55 M	0.55 M	1.0	Ba^{2+}	7	2.5 ml/min
6	0.55 M	0.55 M	1.0	SO_4^{2-}	10	2.5 ml/min
7	0.55 M	0.55 M	1.0	SO_4^{2-}	7	25 ml/s

μCT of Barium Sulfate Nanoparticles

The barium sulfate nanoparticles synthesized using the parameters of Experiment 4 (Table I) were imaged using μCT. A cortical bone specimen was removed from the mid-diaphysis of a bovine tibia using a band saw. Six holes of 1.2 mm diameter and approximately 5.0 mm depth were drilled in the specimen. One hole was used as a control and the other five were filled with

approximately 0.02 ml of aqueous suspensions containing 0.8, 0.6, 0.4, 0.2 and 0.1 vol% barium sulfate nanoparticles. After the water was absorbed by the bone, the specimen was dried and each of the six holes were imaged by μCT (80MG, Scanco Medical AG, Bassersdorf, Switzerland) at 10 μm resolution, 70 kVp voltage, 113 μA current intensity and 200 ms integration time. The image for each hole contained 141 slices (1.4 mm) where each slice was oriented parallel to the depth of the hole. A Gauss filter (sigma = 1; support = 2) was applied to reduce signal noise and a threshold brightness of 17,000 was selected based on the image data from the control hole. All voxels with brightness lower than the threshold were assumed to be cortical bone tissue and filtered off. All voxels with brightness greater than the threshold were assumed to be due to the barium sulfate nanoparticles. Three-dimensional images were constructed using the available software (Image Processing Language, Scanco Medical AG, Bassersdorf, Switzerland).

The minimum detectable thickness of deposited barium sulfate nanoparticles by μCT was also studied. Aqueous suspensions containing 0.2 and 0.1 vol% barium sulfate nanoparticles were prepared and 0.02 ml of each suspension was dropped onto a microscope slide. After the water evaporated, the diameter of the deposited layer was measured, and the thickness of the deposited layer was estimated assuming uniform deposition. Each glass slide was imaged by μCT using the methods described above, with slices normal to the deposited layer and a blank microscope slide as a control for threshold. The thickness of the deposited layer of barium sulfate nanoparticles on each slide was measured from μCT images after threshold.

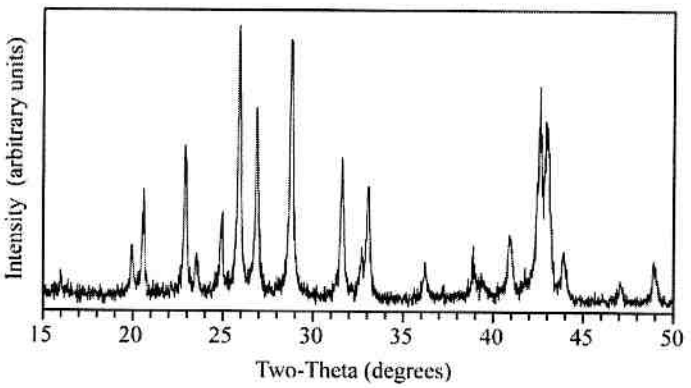

Fig. 1. X-ray diffraction pattern for barium sulfate nanoparticles synthesized with $[Ba^{2+}] = 1.0$ M, $[SO_4^{2-}] = 0.1$ M, SO_4^{2-} feeding, and feeding rate = 2.5 ml/min (Experiment 4).

RESULTS

Synthesis of Barium Sulfate Nanoparticles

XRD patterns identified precipitates from all experimental conditions as barium sulfate.[34] An

exemplary XRD pattern for the barium sulfate nanoparticles prepared by Experiment 4 (Table 1) is shown in Fig. 1. The effects of the experimental parameters on the size and morphology of barium sulfate precipitates were revealed by FESEM. For equimolar amounts of each reagent, increased total reagent concentration resulted in decreased particle size and a more equiaxed morphology (Fig. 2a and b). Particles precipitated at 0.01 M reagent concentrations were plate-like and greater than 1 μm in size. At 0.55 M reagent concentrations, particles were equiaxed and submicron. For a fixed total reagent concentration, increasing the molar ratio of barium to sulfate ions resulted in a substantially decreased particle size (Fig. 2a, c and d). For a molar ratio of 10 (Experiment 4, Table 1), particles were less than 100 nm in diameter. For this powder, the mean particle size measured by XRD line broadening of the (200), (020) and (002) reflections was 52.0 nm, 54.5 nm and 46.3 nm, respectively. Thus, the particles were confirmed to be equiaxed with a mean diameter of approximately 50 nm. All other powders were measured to have mean diameters greater than 100 nm. The feeding reagent also affected the size and distribution of precipitates (Fig. 2a and e). For equimolar amounts of each reagent, particles prepared by sulfate feeding were significantly smaller and more uniform than those prepared by barium feeding. For equimolar amounts of each reagent and sulfate feeding, reduced feeding rate resulted in more uniform precipitates (Fig. 2a and f). The pH of reagent solutions was not shown to significantly affect the size or morphology of precipitates under the conditions investigated.

μCT of Barium Sulfate Nanoparticles

Varying amounts of barium sulfate nanoparticles were deposited in holes drilled in cortical bone tissue and imaged using μCT. Image segmentation at the threshold level of 17,000 removed the entire cortical bone image, and the higher intensity voxels representing barium sulfate were clearly visible (Fig. 3). Images revealed that the particles covered the inner wall of the holes such that the actual thickness of deposited barium sulfate nanoparticles was less than the hole diameter. The measured diameter of holes with deposited barium sulfate nanoparticles was larger than the actual diameter and the measured volume of deposited barium sulfate nanoparticles was larger than the actual volume of deposited particles. The measured volume of barium sulfate nanoparticles was nearly eight times larger than the actual volume (Fig. 4).

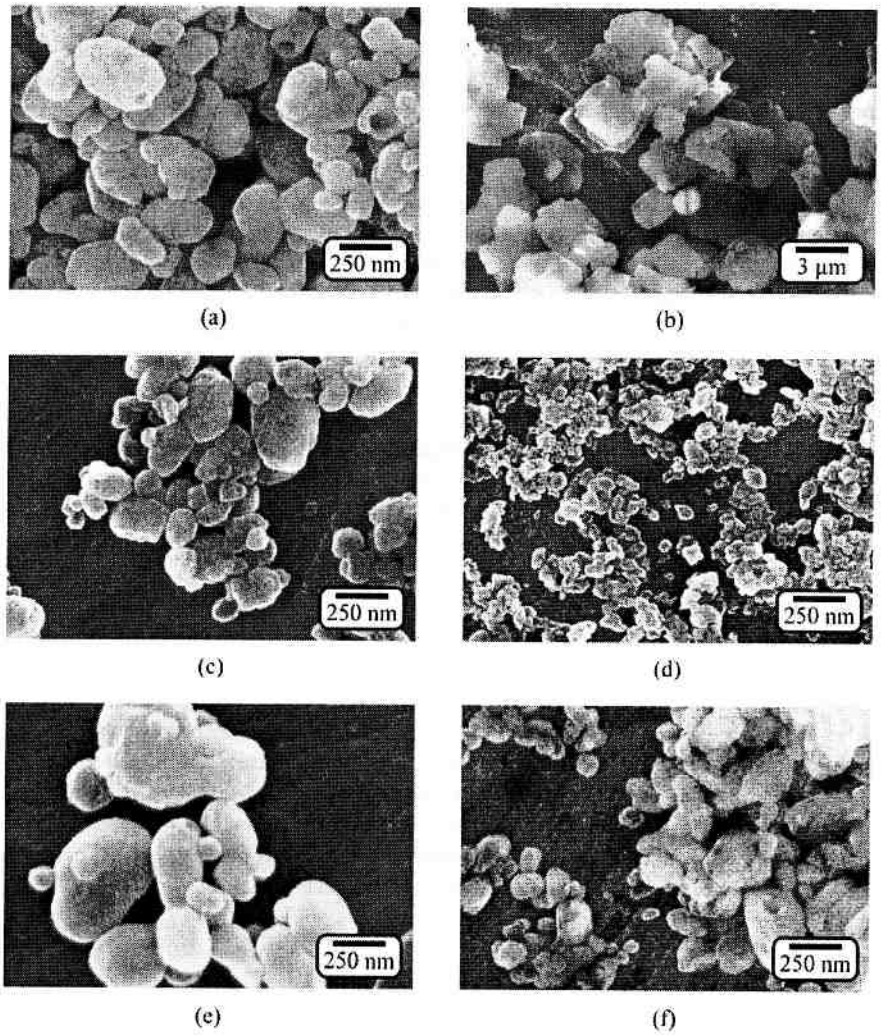

Fig. 2. SEM micrographs of the as-prepared barium sulfate precipitates showing the effects of selected experimental parameters: (a) Experiment 1, $[Ba^{2+}] = [SO_4^{2-}] = 0.55$ M, SO_4^{2-} feeding, feeding rate = 2.5 ml/min; (b) Experiment 2, $[Ba^{2+}] = [SO_4^{2-}] = 0.01$ M, SO_4^{2-} feeding, feeding rate = 2.5 ml/min; (c) Experiment 3, $[Ba^{2+}] = 0.10$ M, $[SO_4^{2-}] = 1.0$ M, SO_4^{2-} feeding, feeding rate = 2.5 ml/min; (d) Experiment 4, $[Ba^{2+}] = 1.0$ M, $[SO_4^{2-}] = 0.1$ M, SO_4^{2-} feeding, feeding rate = 2.5 ml/min; (e) Experiment 5, $[Ba^{2+}] = [SO_4^{2-}] = 0.55$ M, Ba^{2+} feeding, feeding rate = 2.5 ml/min; (f) Experiment 7, $[Ba^{2+}] = [SO_4^{2-}] = 0.55$ M, SO_4^{2-} feeding, feeding rate = 25 ml/s.

Three glass slides with different amounts of deposited barium sulfate nanoparticles were also imaged using μCT. For the 0.2 vol% barium sulfate suspension, the imaged thickness of the barium sulfate layer was 30 μm and the diameter of the layer was about 8 mm, which was almost the same as the measured diameter. For the 0.1 vol% barium sulfate suspension, no layer of pixels was detected. The estimated layer thickness for the 0.2 and 0.1 vol% barium sulfate suspensions was 0.79 μm and 0.24 μm, respectively.

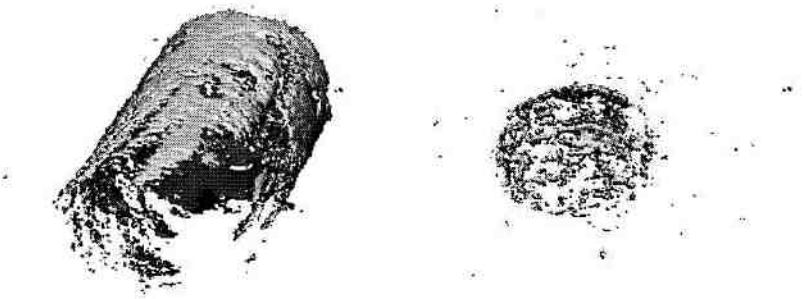

(a) (b)

Fig. 3. Three-dimensional μCT images of barium sulfate nanoparticles deposited from an (a) 0.8 vol% and (b) 0.1 vol% suspension into 1.2 mm diameter holes in cortical bone tissue.

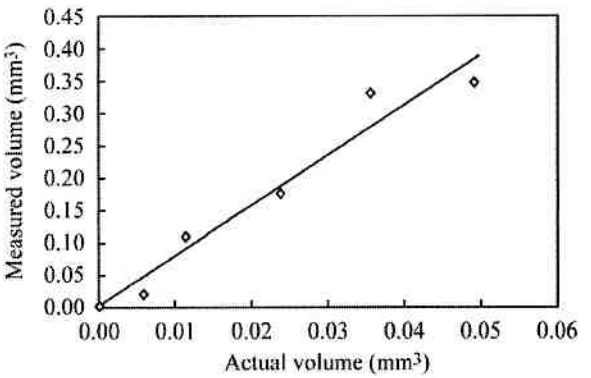

Fig. 4. The relationship between the actual volume of deposited barium sulfate nanoparticles and the volume measured by μCT after threshold. Linear regression of the data yielded $y = 7.75x$ ($R^2 = 0.95$).

DISCUSSION

Synthesis of Barium Sulfate Nanoparticles

The kinetics of precipitation under stoichiometric conditions is well understood. Increasing nucleation rate or decreasing crystal growth rate generally results in smaller precipitates. In this investigation barium sulfate precipitated instantaneously upon mixing the two reagent solutions and the entire system was kept under constant stirring. Therefore, nucleation was expected to govern the precipitate size more than crystal growth. The nucleation rate is influenced by the supersaturation,[18] and the supersaturation ratio, S, is defined as

$$S = \sqrt{[Ba^{2+}][SO_4^{2-}]/K_s} \qquad (2)$$

where the solubility product of barium sulfate is $K_s \approx 1.1 \cdot 10^{-10}$. [24] Thus, increasing total reagent concentration increases the supersaturation and nucleation rate. A higher nucleation rate means that a greater number of stable nuclei form before reaching equilibrium, limiting crystal growth and resulting in a smaller mean particle size.

Accordingly, the results of this study showed that the size of barium sulfate precipitates was reduced from micro-scale to nano-scale by increasing the total reagent concentrations (Fig. 2a and b). A further decrease in particle size was achieved using a molar excess of barium to sulfate (Fig. 2a and d). This result can also be explained by considering the local supersaturation as the sulfate feeding reagent solution was added dropwise to the barium reagent solution. In the case for a molar excess of barium, a higher supersaturation was maintained throughout the duration of precipitation. In other words, the local supersaturation incipient to precipitation was lower for the equimolar reagent solutions, and was governed by the larger volume of the barium reagent solution rather than the droplets of the feeding reagent solution. Furthermore, as barium sulfate precipitated upon mixing the equimolar reagent solutions, the supersaturation decreased rapidly. This decrease in local supersaturation with precipitation was even greater for a molar shortage of barium to sulfate (molar ratio of 0.1). Thus, decreasing molar ratio resulted in an increased variation in the supersaturation during precipitation and a greater variation in the precipitate size distribution (Fig. 2a, c and d). Other investigations have also reported this effect, including a more pronounced effect for a molar excess of barium versus a molar excess of sulfate due to preferential ion adsorption.[18, 24] In order to investigate the latter effect in our system, further experiments are needed where the feeding reagent is reversed for the same molar ratios. Furthermore, the particle size distributions should be quantified in future work. Nonetheless, for equimolar concentrations of barium and sulfate, sulfate feeding resulted in somewhat smaller, more uniform precipitates than barium feeding (Fig. 2a and e), suggesting that a molar excess of barium increased the nucleation rate more than an equal molar excess of sulfate. The increased precipitate size distribution observed for a faster feeding rate (Fig. 2a and f) can be explained by less uniform mixing (greater variation in local supersaturation) for the faster feeding rate. Finally, under the conditions investigated, the solution pH had negligible effect on the supersaturation and therefore showed no effect on the particle size.

μCT of Barium Sulfate Nanoparticles

The results of this study showed the feasibility of detecting barium sulfate nanoparticles in cortical bone tissue using μCT. Furthermore, the results also indicated that barium sulfate nanoparticles influenced adjacent image voxels. The detected signal was amplified by a volumetric factor of nearly eight (Fig. 4). In other words, barium sulfate nanoparticles enabled detection of features smaller than the nominal resolution of the instrument. Currently most commercially available μCT scanners have a resolution on the order of 10 μm and clinical CT scanners have a resolution on the order of 100 μm. Microcracks in bone are typically 30-100 μm in length and no more than 1 μm in width.[1, 12, 13]. Therefore, if barium sulfate nanoparticles can be delivered to microcracks, the amount of barium sulfate nanoparticles or the size of microcracks may have dimensions less than the resolution of the instrument. Moreover, the results from imaging barium sulfate nanoparticles deposited on glass slides indicated a minimum detectable dimension between 0.24 μm and 0.79 μm for barium sulfate nanoparticles using an instrument with 10 μm resolution.

ACKNOWLEDGEMENTS

This work was supported by the National Institutes of Health grant AR 49598.

REFERENCES

[1]R.B. Martin, "Fatigue microdamage as an essential element of bone mechanics and biology," *Calcif. Tissue Int.*, **73** [2] 101-107 (2003).

[2]M. B. Schaffler, E. L. Radin and D. B. Burr, "Mechanical and morphological effects of strain rate on fatigue of compact bone," *Bone*, **10** [3] 207-214 (1989).

[3]M.R. Forwood and A.W. Parker, "Microdamage in response to repetitive torsional loading in the rat tibia," *Calcif. Tissue Int.*, **45**, 47-53 (1989).

[4]D. B. Burr, M.R. Forwood, D.P. Fyhrie, R.B. Martin, M.B. Schaffler and C.H. Turner, "Bone microdamage and skeletal fragility in osteoporotic and stress fractures," *J. Bone Miner. Res.*, **12**, 6-15 (1997).

[5]P. Zioupos and A. Casinos, "Cumulative damage and the response of human bone in two-step loading fatigue," *J. Biomechanics*, **31**, 825-833 (1998).

[6]F.J. O'Brien, D. Taylor and T.C. Lee, "Microcrack accumulation at different intervals during fatigue testing of compact bone," *J. Biomechanics*, **36**, 973-980 (2003).

[7]K.J. Jepsen, D.T. Davy and D.J. Krzypow, "The role of the lamellar interface during torsional yielding of human cortical bone," *J. Biomechanics*, **32**, 303-310 (1999).

[8]D. Vashishth, K.E. Tanner and W. Bonfield, "Fatigue of cortical bone under combined axial-torsional loading," *J. Orthop. Res.*, **19**, 414-420 (2001).

[9]D. B. Burr and M. Hooser, "Alterations to the *en bloc* basic fuchsin staining protocol for the demonstration of microdamage produced *in vivo*," *Bone*, **17**, 431-433 (1995).

[10]T.C. Lee, E.R. Myers and W.C. Hayes, "Fluorescence-aided detection of microdamage in compact bone," *J. Anat.*, **193**, 179-184 (1998).

[11]T.C. Lee, T.L. Arthur, L.J. Gibson and W.C. Hayes, "Sequential labelling of microdamage in

bone using chelating agents," *J. Orthop. Res.*, **18**, 322-325 (2000).

[12]D.B. Burr, C.H. Turner, P. Naick, M.R. Forwood, W. Ambrosius, H. M. Sayeed and R. Pidaparti, "Does microdamage accumulation affect the mechanical properties of bone?," *Journal of Biomechanics*, **31**, 337-345 (1998).

[13]D. Taylor and T.C. Lee, "Measuring the shape and size of microcracks in bone," *J. Biomechanics*, **31**, 1177-1180 (1998).

[14]D.J. Gunn and M.S. Murthy, "Kinetics and mechanisms of precipitation," *Chem. Eng. Sci.*, **27**, 1293-1212 (1972).

[15]M.S. Murthy, "Theory of crystal growth in phase transformations: precipitation of barium sulfate," *Chem. Eng. Sci.*, **49**, 2389-2393 (1994).

[16]K. Taguchi, J. Garside and N.S. Tavare, "Nucleation and growth kinetics of barium sulphate in batch precipitation," *J. Crystal Growth*, **163**, 318-328 (1996).

[17]M.A. vanDrunen, H.G. Merkus and G.M. vanRosmalen, "Barium sulfate precipitation: Crystallization kinetics and the role of the additive PMA-PVS," *Part. Part. Syst. Char.*, **13** [5] 313-321 (1996).

[18]M. Aoun, E. Plasari, R. David and J. Villermaux, "Are barium sulphate kinetics sufficiently known for testing precipitation reactor models?," *Chem. Eng. Sci.*, **51**, 2449-2458 (1996).

[19]M. Aoun, E. Plasari, R. David and J. Villermaux, "A simultaneous determination of nucleation and growth rates from batch spontaneous precipitation," *Chem. Eng. Sci.*, **54**, 1161-1180 (1999).

[20]B. Bernard-Michel, M.N. Pons and H. Vivier, "Quantification, by image analysis, of effect of operational conditions on size and shape of precipitated barium sulphate," *Chem. Eng. J.*, **87**, 135-147 (2002).

[21]M. Yokota, E. Oikawa, J. Yamanaka, A. Sato and N. Kubota, "Formation and structure of round-shaped crystals of barium sulfate," *Chem. Eng. Sci.*, **55**, 4397-4382 (2000).

[22]R. Aguiar, H. Muhr and E. Plasari, "Comparative study of the influence of homogeneous and heterogeneous (multi-phase) precipitation processes on the particle size distribution," *Chem. Eng. Technol.*, **26** [3] 292-295 (2003).

[23]L. Vicum, M Mazzotti and J. Baldyga, "Applying a thermodynamic model to the non-stoichiometric precipitation of barium sulfate," *Chem. Eng. Technol.*, **26**, 325-333 (2003).

[24]D.C.Y. Wong, Z. Jaworski and A.W. Nienow, "Effect of ion excess on particle size and morphology during barium sulphate precipitation: an experimental study," *Chem. Eng. Sci.*, **56**, 727-734 (2001).

[25]A.G. Walton, *The Formation and Properties of Precipitates*, Robert E. Krueger Publishing Co., Huntington, NY, 1979.

[26]S.N. Black, L.A. Bromley, D. Cottier, R.J. Davey, B. Dobbs and J.E. Rout, "Interactions at the organic/inorganic interface: Binding motifs for phosphonates at the surface of barite crystals," *J. Chem. Soc. Faraday Trans.*, **87**, 3409-3414 (1991).

[27]F. Jones, A. Stanley, A.L. Rohl and M.M Reyhani, "The role of phosphonate speciation on the inhibition of barium sulfate precipitation," *J. Crystal Growth*, **29,** 584-593 (2003).

[28]L.A. Bromley, D. Cottier, R.J. Davey, B. Dobbs and S. Smith, "Interactions ate the

organic/inorganic interface: Molecular design of crystallization inhibitors for barite," *Langmuir*, **9**, 3594-3599 (1993).

[29]M. Uchida, T. Sue, A. Yoshioka and A. Okuwaki, "Hydrothermal synthesis of needle-like barium sulfate using a barium(II)-EDTA chelate precursor and sulfate ions," *J. Mater. Sci. Lett.*, **19**, 1373-1374 (2000).

[30]L. Qi, J. Ma, H. Cheng and Z. Zhao, "Preparation of $BaSO_4$ nanoparticles in non-ionic w/o microemulsions," *Colloid Surface A*, **108** 117-126 (1996).

[31]M. Li and S. Mann, "Emergence of morphological complexity in $BaSO_4$ fibers synthesized in AOT microemulsions," *Langmuir*, **16**, 7088-7094 (2000).

[32]J.D. Hopwood and S. Mann, "Synthesis of barium sulfate nanoparticles and nanofilaments in reverse micelles and microemulsions," *Chem. Mater.*, **9**, 1819-1828 (1997).

[33]B.D. Cullity, *Elements of X-Ray Diffraction*, 2nd Edition, Addison-Wesley Publishing Co., Inc., Reading, MA, 1978.

[34]Powder Diffraction File 5-0448, JCPDS-International Center for Diffraction Data (ICDD), 1993.